

USGS MAGELLAN STEREOMAPPING OF VENUS

E. Howington-Kraus, R. L. Kirk, D. Galuszka, B. L. Redding

U.S. Geological Survey, Flagstaff, Arizona 86001 (ahowington@usgs.gov)

Commission 1V, WG IV/7

KEY WORDS: Magellan, Venus, SAR, DTM, Extraterrestrial Mapping

ABSTRACT:

This paper describes our methods for generating high resolution Digital Terrain Models (DTMs) of Venus using Magellan synthetic aperture radar (SAR) stereoimages, and the sensor model we developed for Magellan stereomapping on our digital photogrammetric workstation running SOCET SET (® BAE SYSTEMS). In addition to demonstrating the validity of our sensor model and procedures we use for mapping, we explain potential error sources that we have identified as well. We also present test results of our ability to produce DTMs using opposite-side Magellan stereo. This capability can compliment normal same-side stereomapping in areas of low relief by providing exaggerated stereo helpful for DTM generation, and by providing a source of stereo information in gaps occurring in the nominal Magellan stereocoverage.

1. INTRODUCTION

The Magellan spacecraft went into Venus orbit in 1990 and by 1992 had made three complete cycles of polar orbits, each cycle covering the full range of longitudes. During this time the spacecraft obtained a total of 4225 usable synthetic aperture radar (SAR) images of >96% of the planet at a resolution of 75 m/pixel (Saunders et al., 1992). Images taken with a decreased look angle from vertical, primarily during Cycle 3, provide stereo coverage of 17% of the planet when combined with images with same-side illumination from earlier in the mission (primarily in Cycle-1). The stereo geometry of these images is extremely favorable, allowing elevation measurements with an estimated vertical precision (EP) of ~10 m (Leberl et al., 1992). Opposite-side coverage was obtained over a greater area with even stronger stereo geometry, and can be useful in mapping areas of low relief such as the lowland plains. Magellan also obtained radar altimetry data at a horizontal resolution of 10x25 km, but photogrammetric analysis of the stereoimagery can yield topographic maps with a horizontal resolution more than an order of magnitude superior to that of the altimeter.

2. MAGELLAN SAR DATA

The raw SAR data was processed to create Basic Image Data Records (BIDRs) which contain a full set of ancillary data associated with the imagery. Full-resolution Basic Image Data Records (F-BIDRs) are long, thin strips of radar imagery (or “noodles”) that represent one orbit of the Magellan spacecraft. The F-BIDRs are in Sinusoidal map projection and typically cover an area ~20 km wide by 17,000 km long. Because F-BIDRs are difficult to use for geologic interpretation, they have been mosaicked in the various formats shown in table 1.

Mission mosaicked F-MIDRs (Full-resolution Mosaicked Image Data Records), mission mosaicked C-MIDRs (Compressed Mosaicked Image Data Records), and USGS FMAPS are also in

Sinusoidal map projection. The C-MIDRs were created by compressing the F-MIDRs to form lower resolution but larger area mosaics; however, the F-MIDRs do not include the complete set of F-BIDRs, therefore the USGS Astrogeology Team produced the FMAP series which was created from the entire set of available Magellan F-BIDRs. (Batson et al., 1994).

Mosaic Product	Resolution (m)	Coverage
F-MIDR	75	5°x5°
C1-MIDR	225	15°x15°
C2-MIDR	675	45°x45°
C3-MIDR	2025	120°x80°
FMAP	75	12°x12°

Table 1: Resolution and area of coverage of Magellan mosaicked products.

3. APPROACH

Our approach to Magellan stereomapping is the coupling of our in-house planetary image and cartographic processing package, ISIS (Eliason, 1997; Gaddis et al., 1997; Torson and Becker, 1997), with our digital photogrammetric workstation running SOCET SET (® BAE SYSTEMS) (Miller and Walker, 1993; 1995). ISIS (Integrated Software for Imagers and Spectrometers) and photogrammetric systems parallel each other in many respects: both import/export and processes images, have bundle-block adjustment capabilities, and produce cartographic products. ISIS has mission-specific data ingestion and calibration software, along with a suite of special purpose application software, however it does not have stereoprocessing capabilities. The special hardware and SOCET SET (SoftCopy Exploitation Tool Set) software of our photogrammetric system provide many useful capabilities for mapping, including import/export of common data formats, multi-sensor bundle-block adjustment, automatic extraction of DTM data, stereo display and interactive editing of DTMs, orthophoto generation and mosaicking, and image display and enhancement tools.

These capabilities can be extended by programming with the SOCET SET Developer's Toolkit (DEVKIT). While commercial off-the-shelf digital photogrammetric systems cannot handle most planetary data, software changes in only two areas are needed for them to do so: 1) input/output of planetary image data and supporting geometric information, and 2) development of "sensor models" specifying the transformation between image lines/samples and object space for the variety of planetary sensors. For several planetary missions, all that is required for stereomapping are programs to import planetary images and supporting data from ISIS into SOCET SET, however the unique properties of the Magellan SAR data made it necessary to develop both translation software and a sensor model (Howington-Kraus et al., 2000).

4. SENSOR MODEL

A sensor model is a function that specifies the transformation between image space (lines, samples) and object or ground coordinates (latitude, longitude, elevation). Our Magellan SAR sensor model is rigorous and flexible. It includes all the physics of the Magellan imaging process, and accounts for the fact that during the imaging process, the images have been partially orthorectified as part of the correlation process: distortions attributable to topography were removed (but only those accounted for in the very low resolution pre-Magellan topo model) and must be put back in for the images to be matched correctly. The sensor model is designed to work with any combination of unmosaicked (F-BIDR), Mission-mosaicked (F- and C-MIDR), and USGS-mosaicked (FMAP) images. Information about the spacecraft position and velocity can be taken either from the BIDR headers or from separate NAIF SPICE kernels, letting us take advantage of post-mission improvements to the spacecraft ephemerides. In addition, the SOCET SET bundle-adjustment software can be used to estimate corrections to the ephemeris of each orbit. The form of the corrections, offsets in three orthogonal directions (along-track, across-track, and radial) suffices to correct the orbits over short arcs and reconcile SAR and altimetry observations.

5. PROCEDURES

5.1 Data Import

For a selected site, the Cycle-1 and Cycle-3 F-BIDRs and FMAP mosaics covering the map area are identified and ingested into ISIS. (Because F-BIDRs cover the full range of latitude, only the portion of imagery needed for the map area is extracted.) Additionally, for each F-BIDR, the necessary support data are retrieved from the BIDR libraries and NAIF SPICE kernels, as needed, and stored in a database accessed by the sensor model. (Populating the database is done on a one-time basis per BIDR for the entire length of the orbit.)

Two sources of spacecraft ephemerides are available: the mission ephemerides and improved ephemerides computed by Alex Konopliv of JPL based on the gravity model available at the end of the Magellan mission (Rappaport et al., 1999). For reasons described below, we retrieve the Konopliv ephemerides

from the NAIF SPICE kernels, while all other support data is retrieved from BIDR headers. Starting with Konopliv ephemerides, all Cycle-1 and Cycle-3 F-BIDRs contained in a map area are then imported into SOCET Set.

In addition to the image and support data, the gridded Magellan altimetry is also needed for mapping. ISIS is used to extract the portion of the altimetry data that encompasses the map area, and other software is then used to convert the results into an ASCII ARC/INFO GRID for import into SOCET Set.

5.2 Bundle Adjustment

Starting with the improved ephemerides computed by Konopliv plus control points constrained to reliable Magellan altimetry measurements, we further adjust individual F-BIDRs to minimize the image-to-image and control-to-altimetric-elevation discrepancies. Measuring image points and performing the adjustment calculations must be done with single-orbit (BIDR) data so that each strip of imagery is free to be adjusted separately (and because mosaics do not preserve all image information in the overlap areas of interest). Because the F-BIDRs are adjusted rigidly in three axes, the images/stereomodels will not "bend" to accommodate inconsistencies in the altimetry data. Therefore, ties with inconsistent altimetry data are easily detectable and not used as elevation constraints in our bundle-block adjustment. Once the adjustment process is acceptable, the FMAP mosaics are imported with Konopliv ephemerides plus our adjustments, thereby allowing mapping to proceed with mosaics.

5.3 DTM Collection

Automatic DTM generation is achieved using SOCET Set's Automatic Terrain Extraction (ATE) tool (Zhang and Miller, 1997). DTM extraction is performed primarily from FMAP mosaics, but in potential problem areas within a mosaic, where pixels are lost at F-BIDR seams, we resort to extracting DTMs from the unmosaicked F-BIDRs. For full-resolution (75 m/pixel) Magellan imagery, we generate DTMs at a post spacing of 675 meters (or 9 pixels) because the noisy radar data are likely to need more averaging and produce more erroneous matches than would optical images. However, a practical lower limit for independent elevation measurements of 225 m, corresponding to a 3-pixel matching window, could be achieved at the expense of additional computation and manual editing time. (DTM posts could be placed closer together than this but smaller topographic features would not be resolved.)

Prior to running ATE, we "seed" the DTMs with manually collected points on ridge and valley lines, or with reliable altimetry data. This greatly improves the success rate of the automatic matching step, and generally limits the need for manual editing to bland areas, where the matcher fails entirely, and to 'blunders' found at the image edges where elevation values are extrapolated.

Interactive editing is done next, again primarily from the FMAP mosaics, but we resort to the single-orbit F-BIDR's so that mismatches in mosaicked products are not propagated into the DTM. After interactive editing, individual DTMs are combined

into a single DTM for the entire map area. The merged DTM then requires additional interactive editing to replace gaps (due to missing data in orbits) with corresponding altimetry data.

5.4 Cartographic Products

The edited and altimetry-merged DTMs are our primary output product, from which we produce various derived products such as orthorectified images, topographic maps and color-coded shaded relief images. All digital products are compatible with ISIS and the ARC/INFO GIS (Geographic Information Systems) suite as well.

When mapping with FMAP mosaics, we produce 1:1,500,000-scale topographic maps, at a contour interval of 200 meters, with orthomosaic base, nomenclature, and collar information. We also produce color-coded shaded-relief/elevation maps because they portray subtle topographic relations that assist with analyses of tectonic deformation, stratigraphic interpretation, flow direction, mass wasting, etc. The color-coding is chosen to show as much information as possible within a given map area, and hence is not necessarily consistent planetwide.

6. VALIDATION

6.1 Ephemeris Corrections

We first addressed the well-known "cliffs," artifacts in the stereo data caused by discrepancies between the mission ephemeris solutions for successive blocks of orbits. As mentioned previously, Alex Konopliv reprocessed the entire set of orbital tracking and navigation data based on the detailed gravity observations from the end of the mission and claimed that errors in the new orbit solutions were decreased 1.5 orders of magnitude (to 50-200 m) in all 3 axes. Our test mapping unfortunately showed that errors of this magnitude north-south interfered with stereomatching, while east-west ephemeris errors resulted in height offsets in the derived stereomodels. To produce seamless elevation data, we found it necessary to collect image-to-image tie point measurements and use these to estimate local position corrections to the orbits. Correcting the Konopliv ephemerides in this way yields solutions in good agreement with Magellan altimetry. (Correcting the mission ephemerides eliminates relative errors (seams) between stereomodels but does not correct the absolute positional errors present in the earlier solution.) We concluded that both the improved orbit/tracking solution and corrections based on the images themselves are necessary for successful stereomapping.

6.2 Insensitivity to Altimetry Artifacts

Our adjustment calculation takes as input both the coordinates of selected features (control-points) in the images and interpolated Magellan altimetry data. The resulting corrections to the ephemerides are intended not only to make the overlapping same-cycle images align seamlessly, but to make the elevations of pass-points calculated from stereo agree with the elevations from altimetry. Because elevations of individual altimeter footprints can be in error by several kilometers at

high-contrast boundaries in the surface scattering function, the question arose of how sensitive our bundle adjustment process is to artifacts in the Magellan altimetry.

The most direct verification of our results would have been a comparison of our DTMs with independent, non-Magellan derived elevation data. Unfortunately, the best Earth-based elevation dataset for Venus, derived from Goldstone radar observations (Jurgens et al., 1980), was insufficient to address the potential errors inherited from Magellan altimetry. Only three altimetric observations by the Goldstone radar overlap with the Magellan stereo coverage. The nominal resolution of these DTMs is 1 to 5 km horizontally and 15 to 60 m vertically, but they are dominated by artifacts and noise with a standard deviation of 1 km or more. It is difficult, if not impossible, to identify known topographic features in these DTMs. In addition, the data are not tied precisely to the Magellan coordinate system. We therefore did not attempt to map the corresponding regions in order to compare our results to the Goldstone DTMs. As a result, an indirect approach to validating our results was required.

The temperature- and therefore elevation-dependence of radar backscatter properties on Venus provided a means to demonstrate that the sensor model's adjustable parameters allow each image to be translated and rotated as a whole, but not to be "warped" to fit erroneous altimetry data. Low-reflectivity lowlands give way to extensive bright highlands, with a few of the highest elevations once again radar-dark. The lower transition occurs over a relatively broad range of elevations locally and at a height that varies by several kilometers globally. The upper transition is noticeably sharper and was therefore selected for test mapping. In particular, we mapped the portion of central Ovda Regio from 88-98E longitude, 8-5S latitude (Figure 1), which contains several high-elevation dark regions.

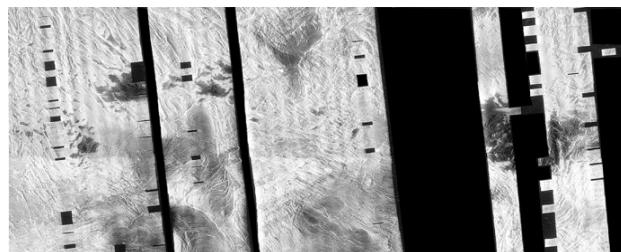


Figure 1. Portion of central Ovda Regio selected for topographic mapping tests. Boundaries of dark patches indicate thermochemical transition that should occur at near-constant elevation. Region is 88-98E longitude, 8-5S latitude. Data are taken from Cycle 3 (stereo look angle) C1-MIDR photoproducts. Not all orbits seen here were included in FMAP mosaics or could be found in F-BIDR archives, so area stereomapped is less complete.

Images (F-BIDRs) used for our mapping came from 47 Cycle-1 orbits in the range 0947-0994 and 34 Cycle-3 orbits in the range 4536 to 4582; some images present in the Magellan Mission C1-MIDR mosaics were not used because they were not present in the USGS FMAP or because data were missing from the archive of F-BIDRs. Control points, 212 in all, were interactively measured between neighboring images of the same

cycle, and between overlapping Cycle-1 and Cycle-3 images where possible. Because of gaps in the Cycle-3 data, it was not possible to connect all images by points that could be measured on both cycles (i.e., in stereo). Elevations of the control points were constrained based on the Magellan altimetry, and a least-squares bundle-block adjustment of the spacecraft ephemerides was performed to minimize the image-to-image and control-to-altimetric-elevation discrepancies. In this adjustment, constant offsets in the three orthogonal directions (along-track, across-track, and radial) were applied to the spacecraft orbit arc for each image. Higher-order deformation of the orbits was not modeled. Altimetric elevations inconsistent with the remainder of the altimetry data and the stereoimagery were readily identifiable because they produced large elevation residuals. Control points found in this way to be tied to unreliable altimetry data were eliminated from the final control solution. Where possible, they were replaced by control points nearby for which elevation residuals were found to be acceptable. After a satisfactory control solution was obtained, DTMs were collected by automatic stereomatching of each overlapping stereopair of images. A bare minimum of interactive editing was done to correct spikes in a few areas where the automatic matcher failed.

A closeup of our contour data (Figure 2) shows that the margin of the dark regions varies locally in elevation by <200 m for considerable distances. The elevation of the bright-dark transition varies by a maximum of 500 m across the entire region we mapped. A few areas on the right of Fig. 2 that appear dark but are several hundred meters lower are probably unrelated to the reflectivity change with altitude. They appear smooth at the resolution of the image, and, if they are also smoother than their surroundings at the scale of the radar wavelength, this would explain their dark appearance.

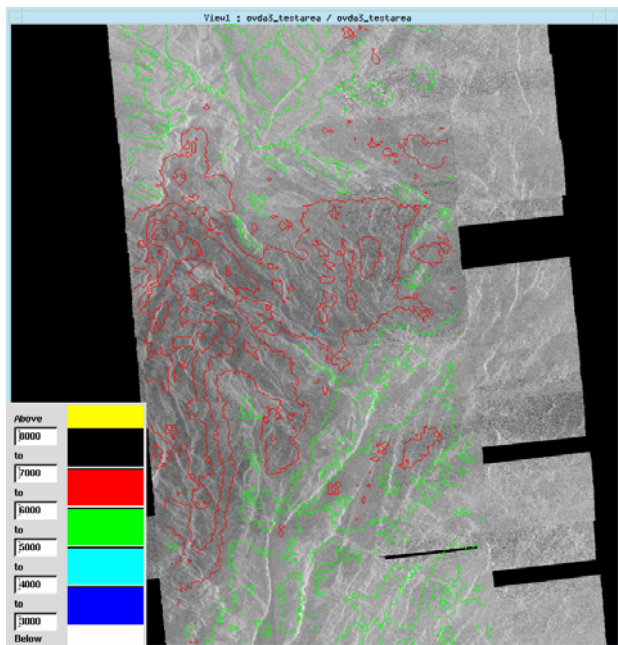


Figure 2. Closeup of contours derived from stereo DTM for part of the region shown in Fig. 1, centered near -7° lat, 96° lon. Contour interval is 250 m, with contours colored by absolute

elevation as shown. Elevation along boundary of largest dark patch is constant to <200 m.

In contrast to our stereo-derived DTM (Figure 3), the Magellan altimetry for this area shows a series of apparent "pits" 20-50 km wide (i.e., one to a few altimetry footprints) and typically 3 km deep. A chain of such pits runs through the dark areas; if the altimetry were correct, some of the dark material would have to lie 3 km below the majority of the transition boundary. Furthermore, local slopes of as much as 15 degrees would be implied; there is no morphologic evidence for such slopes in the images or for any visible peculiarity spatially associated with the altimetry lows. We conclude that these low elevations are artifacts resulting from noisy or incorrectly interpreted altimeter echos. Fortunately, the vast majority of the altimetry data are not subject to such severe errors, so it is possible to constrain the stereogrammetric control solution to follow the altimetric DTM where it is valid and robustly exclude bad altimetry datapoints from the control solution.

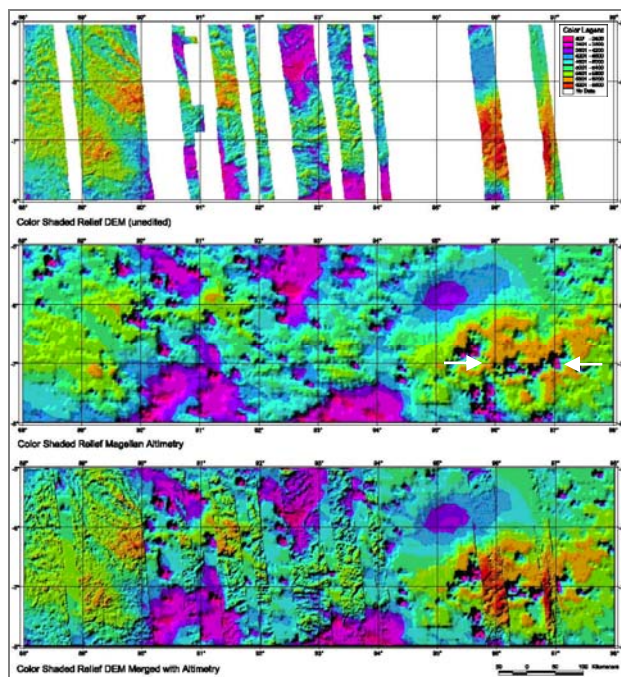


Figure 3. Digital Terrain Models (DTMs) of region shown in Figure 1. From top to bottom: color-coded shaded relief computed from stereo; color shaded relief from Magellan global gridded altimetry dataset; stereo data merged with altimetry. Stereo data were collected at 675 m (9 pixel) post spacing, whereas altimetry footprint size is >10 km and track spacing is ~25 km. Altimetry dataset also contains prominent errors (e.g. near -7° lat, 95° - 97° lon; shown between white arrows on center panel) in the form of incorrect low elevations ("pits") near boundaries of radar-dark patches. These errors are not reflected in stereo DTM because erroneous altimetry data were identified and excluded from the bundle-adjustment calculation.

Our DTM results do not show any sign of the multi-kilometer depressions seen in the altimetric DTM for this area. We were easily able to detect during our bundle-adjustment process that the altimetric elevations in the apparent depressions were inconsistent with the remainder of the data and therefore did not use these elevations as constraints in the calculation. The result

of our bundle-adjustment with selective use of altimetry constraints and the other software and procedures we have developed is a high-resolution, stereo DTM that agrees well with altimetry in the regions of uniform reflectivity where it is reliable yet is not distorted by the altimetry artifacts where there are strong reflectivity contrasts.

6.3 Residual Coordinate Discrepancy

Finally, we found that the north-south coordinates of burst center points computed in our sensor model differed from the values stored in the F-BIDR headers. We traced this coordinate discrepancy, which is negligible at low latitudes and up to <2 pixels (0.15 km) at high latitudes, to the difference between implementations of the atmospheric refraction correction in our software and in the Magellan UNIX SAR Processor (USP) that produced the BIDRs. Both software packages use a simple empirical function fit to numerical calculations of atmospheric refraction. It seems likely that our calculation, which uses a rational function of ground point elevation, spacecraft elevation, and their horizontal separation, is slightly more accurate than the SAR processor code, which uses a polynomial in spacecraft elevation and horizontal separation only. Nevertheless, we attempted to adopt the USP atmospheric refraction code in our sensor model for consistency with the F-BIDR headers. Problems with the USP code became apparent when trying to correct F-BIDRs with significant along-track offsets during bundle adjustment. The doppler calculations in the USP code is not sensitive to shifts in the spacecraft position which resulted in stereomodels for which y-parallax (a misalignment of the images in the north-south direction) could not be removed. We therefore reverted back to our original version of the sensor model because it works in the bundle adjustment.

7. USE OF OPPOSITE-SIDE STEREO

To exploit all available information in the Magellan SAR dataset, we evaluated our potential to map Venusian plains using Magellan opposite-side (right-look/left-look) stereopairs. For normal stereomapping, same-side (left-look/stereo-look) stereopairs are used because the opposite illumination of right- and left-look stereopairs makes it difficult to map the highlands. Image contrast in these rugged areas comes primarily from topographic shading of slopes, which appears reversed in the opposite-side illuminated imagery. However opposite-side stereopairs provide exaggerated stereo helpful for data collection in bland Venus plains, and they can serve as potential gap-fill in the stereo-look coverage. Image contrast in these areas of low relief comes primarily from intrinsic variations in backscattering properties, and hence is not reversed under opposite-side illumination.

To demonstrate our mapping capabilities with opposite-side stereo, we chose a test area in the Joliot-Curie FMAP quadrangle (06S066). A total of 29 F-BIDRs covered the test area: 12 left-look (Cycle-1) F-BIDRs in the range 0829-0840, 6 right-look (Cycle-2) F-BIDRs in the range 2643-2648, and 11 stereo-look (Cycle-3) F-BIDRs in the range 4416-4429. Following our nominal mapping procedures, we performed a

bundle adjustment of the individual F-BIDRs, and applied the ephemeris corrections to mosaics covering the test area. We next collected corresponding DTMs of terrain indicative of Venusian plains by automatically stereomatching the same region using same-side and opposite-side stereopairs, and we made no edits of the results (Figure 4). (Because of the known difficulty of matching opposite-side radar images in rugged terrain as described above, we made no attempts to map highland areas.) Other than the image source, both DTMs had identical input parameters for ATE, including the seeded DTM.

The same-side results contain several types of artifacts attributable to matcher errors. These artifacts include polygonal regions of sharply differing elevation (visible as closely spaced sets of straight contour segments), ridges whose existence is not supported in the imagery, and a trough-like representation of

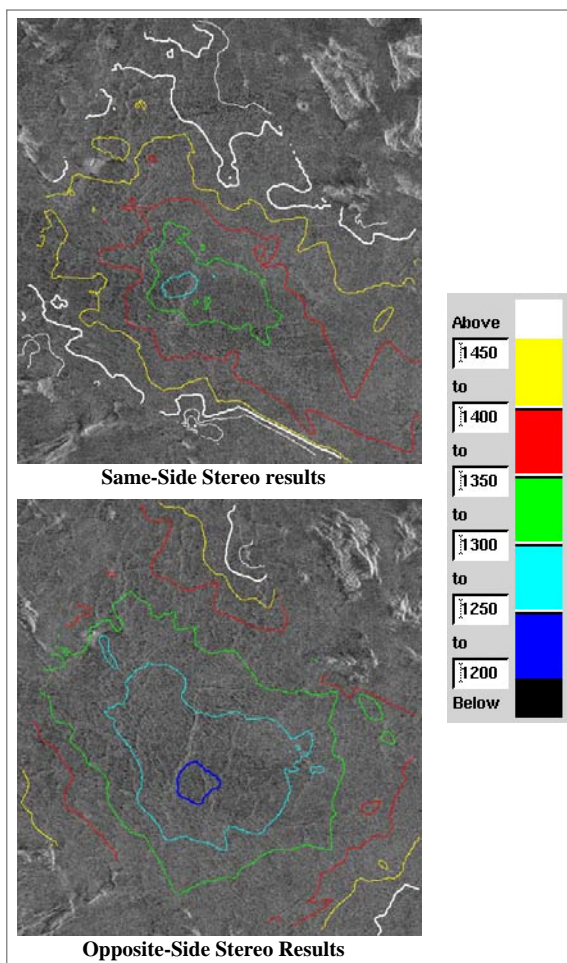


Figure 4: Closeup of contours derived from Same-Side and Opposite-Side stereomatching results over the same portion of FMAP quadrangle Joliot-Curie. Contour interval is 50 m, with contours colored by absolute elevation as shown. Top panel shows same-side results (Left Look / Stereo Look), overlaid on the left-look image base. Bottom panel shows opposite-side (Right Look / Left Look) results, overlaid on the right-look image base.

the depression area. In contrast, the character of the opposite-side results are indicative of successful stereomatching, and

only isolated matcher artifacts exist primarily where the DTM boundary borders features with some relief. There is a 50 m elevation shift between the same- and opposite-side stereo results evident in the depression area, however, when viewing the results in stereo, the same-side contours appear to be floating above the stereomodel surface, while the opposite-side contours appear to hug the surface. This leads us to conclude that the matcher was not locked onto ground in the same-side stereopair, and the exaggerated stereo of the opposite-side stereomodel aided the matching process to achieve more accurate results.

8. CONCLUSION

The results of our stereomapping process are high-resolution stereo DTMs that agree well with the Magellan altimetry, where the altimetry is reliable, yet are not distorted by altimetry artifacts. The horizontal resolution of these products improves dramatically on the altimetry as well. To date we have generated maps of the 12°x12° FMAP quads Joliot-Curie (Figure 5) and Greenaway (both in publication), and a test area in Ovda Regio. Although NASA is not currently funding the systematic collection of additional DTMs of FMAP quads, the capabilities described here remain available for potential special area mapping.

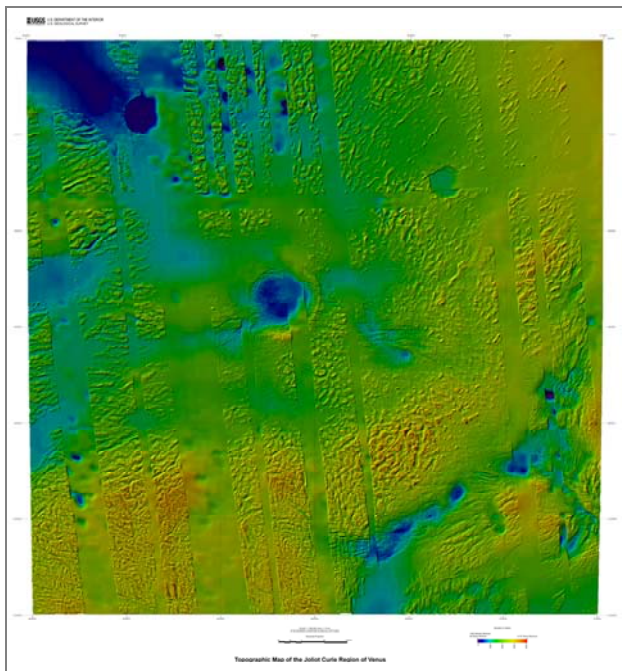


Figure 5: Example output product: color-coded shaded relief map of the Joliot-Curie (06S066) FMAP quadrangle. Stereo data were collected at 675 m post spacing, edited to correct errors introduced during automatic stereomatching, and merged with gridded Magellan altimetry.

9. REFERENCES

- Batson, R.M., Kirk, R.L., Edwards, K.F., and Morgan, H.F., 1994. Venus cartography: *Journal of Geophysical Research*. 99, pp. 21,173–21,182.
- Eliason, E., 1997. Production of digital image models using the ISIS system. *Lunar and Planetary Science*, XXVIII, pp. 331–332.
- Gaddis, L.R., Anderson, J., Becker, K., Becker, T., Cook, D., Edwards, K., Eliason, E., Hare, T., Kieffer, H., Lee, E.M., Mathews, J., Soderblom, L., Sucharski, T., and Torson, J., 1997. An overview of the Integrated Software for Imaging Spectrometers (ISIS). *Lunar and Planetary Science*, XXVIII, pp. 387–388.
- Howington-Kraus, E., Kirk, R., Galuszka, D., Hare, T., and Redding, B., 2000. Rigorous sensor model for topographic mapping of Venus using Magellan radar stereoimagery. *Lunar and Planetary Science*, XXXI, Abstract #2061, Lunar and Planetary Institute, Houston (CD-ROM).
- Jurgens, R.F., Goldsetein, R.M., Rumsey, H.R., and Green, R.R., 1980. Images of Venus by three-station interferometry—1977 results. *Journal of Geophysical Research*, 85(A13), pp. 8282–8294.
- Leberl, F.W., Thomas, J.K., and Maurice, K.E., 1992. Initial results from the Magellan Stereo Experiment. *Journal of Geophysical Research*, 97(E8), pp. 13,675–13,689.
- Miller, S.B., and Walker, A.S., 1993. Further developments of Leica digital photogrammetric systems by Helava. *ACSM/ASPRS Convention and Exposition Technical Papers*, 3, pp. 256–263.
- Miller, S.B., and Walker, A. S., 1995. Die Entwicklung der digitalen photogrammetrischen Systeme von Leica und Helava. *Zeitschrift für Photogrammetrie und Fernerkundung*, 63(1), pp. 4–16.
- Rappaport, N.J., Konopliv, A.S., Kucinskas, A.B., and Ford, P.G., 1999. An improved 360 degree and order model of Venus topography. *Icarus*, 139, pp. 19–31.
- Saunders, R.S., et al., 1992. Magellan Mission Summary. *Journal of Geophysical Research*, 97(E8), pp. 13,067–13,090.
- Torson, J., and K. Becker, 1997. ISIS: A software architecture for processing planetary images. *Lunar and Planetary Science*, XXVIII, pp. 1443–1444.
- Zhang, B., and Miller, S., 1997. Adaptive Automatic Terrain Extraction. *Proceedings of SPIE, Volume 3072, Integrating Photogrammetric Techniques with Scene Analysis and Machine Vision* (edited by D. M. McKeown, J. C. McGlone and O. Jamet). pp. 27–36.